β decay studies of the neutron-rich ^{56,57,58}V isotopes

P.F. Mantica[1,2], A.C. Morton[1], B.A. Brown[1,3], A.D. Davies[1,3], T. Glasmacher[1,3], D.E. Groh[1,2], S.N. Liddick[1,2], D.J. Morrissey[1,2], W.F. Mueller[1], H. Schatz[1,3], A. Stolz[1], S.L. Tabor[4], M. Honma[5], M. Horoi[6], and T. Otsuka[7]

(1) *National Superconducting Cyclotron Laboratory, Michigan State University, East Lansing, Michigan 48824 USA*

(2) *Department of Chemistry, Michigan State University, East Lansing, Michigan 48824 USA*

(3) *Department of Physics and Astronomy, Michigan State University, East Lansing, Michigan 48824 USA*

(4) *Department of Physics, Florida State University, Tallahassee, Florida 32306 USA*

(5) *Center for Mathematical Sciences, University of Aizu, Tsuruga, Ikki-machi, Aizu-Wakamatsu, Fukushima 965-8580, Japan*

(6) *Physics Department, Central Michigan University, Mount Pleasant, Michigan 48859 USA and*

(7) *Department of Physics, University of Tokyo, Hongo, Tokyo, 113-0033 and RIKEN, Hirosawa, Wako-shi, Saitama, 351-1098 Japan*

(Dated: November 11, 2002)

Abstract

β decay of ^{56,57,58}V has been used to populate low-energy levels of ^{56,57,58}Cr, respectively. The low-energy levels of the even-even Cr isotopes and β-decay half-lives and branching ratios of the parent V isotopes are compared to results of shell model calculations. The Cr energy level calculations were completed in the full pf-model space, using several different interactions. The systematic variation of $E(2_1^+)$, which is indicative of a subshell closure at $N = 32$, was best reproduced in calculations using the GXPF1 interaction.

INTRODUCTION

The first excited 2^+ state, $E(2_1^+)$, in $^{52}_{20}Ca_{32}$ has energy 2.56 MeV [1], well above that observed in its even-even neighbor, $^{50}Ca_{30}$. The increase in $E(2_1^+)$ for ^{52}Ca was attributed to a filled neutron $2p_{3/2}$ single-particle orbital, suggesting a significant subshell closure at $N = 32$. An increase in binding at ^{52}Ca was also inferred from a measurement of the mass of this nuclide [2]. It has been proposed that a neutron spherical subshell closure at $N = 32$ could occur when reinforced by the $Z = 20$ proton shell closure [3]. However, an $E(2_1^+)$ of 1007 keV in $^{56}_{24}Cr_{32}$ is also above that observed for its even-even neighbor, $^{54}Cr_{30}$. The systematics of the first excited 2^+ states in the Cr isotopes are shown in Fig. 1, where data are taken from Refs. [4–6]. A peak in the systematic variation of $E(2_1^+)$ at ^{56}Cr, which has four protons in the $1f_{7/2}$ orbital, has been confirmed by the recent measurement of the first excited 2^+ state in $^{58}Cr_{34}$ [4, 7].

The appearance of the $N = 32$ subshell closure for neutron-rich nuclides has been attributed to a diminished $\pi f_{7/2}$ - $\nu f_{5/2}$ monopole interaction as protons are removed from the $1f_{7/2}$ single-particle orbital [7]. The shift in the energy of the $f_{5/2}$ single-particle strength between the $N = 29$ isotones $^{49}_{20}$Ca and $^{57}_{28}$Ni is illustrated in Fig. 2. The levels in Fig. 2 are labelled with their normalized spectroscopic factors (C^2S) based on the single-neutron transfer data compiled in Refs. [8, 9]. In ^{49}Ca, which has an empty $\pi 1f_{7/2}$ orbital, the $5/2_2^-$ state carries most of the $f_{5/2}$ single-particle strength and is nearly 4 MeV above the $3/2^-$ ground state. The $5/2_1^-$ state at 768 keV excitation energy carries the $f_{5/2}$ single-particle strength in ^{57}Ni. With eight protons occupying the $1f_{7/2}$ orbital in ^{57}Ni, the $f_{5/2}$ single-particle state is lowered by more than 3 MeV compared to ^{49}Ca. This large shift in the position of the $f_{5/2}$ single-particle state can be contrasted with the small change in position of the $1/2_1^-$ state, which carries nearly all the $p_{1/2}$ single-particle strength, between ^{49}Ca and ^{57}Ni. The migration of the $\nu f_{5/2}$ single-particle orbital to higher energies with the removal of protons from the $1f_{7/2}$ orbital, in concert with a significant spin-orbit splitting between the $\nu p_{3/2}$ and $\nu p_{1/2}$ orbitals, gives rise to a subshell closure at $N = 32$.

In this paper, we report the low-energy structures of ^{56,57,58}Cr populated following β decay of ^{56,57,58}V, respectively. The neutron-rich Cr isotopes have the highest Z value of nuclides showing evidence for a substantial subshell gap at $N = 32$. A first study of the β-decay properties of ^{56,57,58}V was completed by Sorlin *et al.* [10]; in addition to decay lifetimes,

β-delayed γ-ray spectra were obtained for these nuclides using a high-efficiency BGO array. β-decay half-lives for ^{56,57,58}V were also measured by Ameil *et al.* [11] and compare favorably with those in Ref. [10]. Results from our initial study of the β decay of ^{58}V produced via fragmentation of a 70 MeV/nucleon ^{70}Zn beam were reported in Refs. [4, 7].

EXPERIMENTAL TECHNIQUE

The β-decay parents of interest were produced by intermediate-energy projectile fragmentation using the experimental facilities at the National Superconducting Cyclotron Laboratory (NSCL) at Michigan State University. A primary beam of ^{86}Kr was accelerated to 140 MeV/nucleon using the Coupled Cyclotron Facility as follows: a low-energy beam of $^{86}Kr^{14+}$ from the Superconducting Electron Cyclotron Resonance Source was first accelerated to 12.2 MeV/nucleon using the K500 Superconducting Cyclotron and, following foil stripping to produce $^{86}Kr^{34+}$, accelerated to full energy in the K1200 Superconducting Cyclotron. The average primary beam current was 3 pnA, as measured with a shielded Faraday cup at the target position of the A1900 fragment analyzer. The primary beam was fragmented in a 376-mg/cm^2 thick Be target located at the object position of the A1900. A 330 mg/cm^2 Al degrader was placed at the intermediate image of the A1900 to separate fully-stripped fragment isotopes with given mass-to-charge ratio based on A and Z. The momentum acceptance was set to 1% using a fixed slit also placed at the A1900 intermediate image. A radioactive beam containing ^{54}Sc (1%), ^{55}Ti (14%), ^{56}V (24%), ^{57}V (26%) and ^{58}Cr (34%) was obtained with the A1900 magnetic rigidities set to $B\rho_1 = 4.0417$ Tm and $B\rho_2 = 3.7554$ Tm. A second set of magnetic rigidities, $B\rho_1 = 4.1261$ Tm and $B\rho_2 = 3.8417$ Tm, provided the isotopes ^{55}Sc (0.5%), ^{56}Ti (12%), ^{57}V (38%), ^{58}V (39%) and ^{59}Cr (29%).

Secondary fragments were sent to the NSCL β counting system [12] located in the S1 experimental vault. The Si detector arrangement for the counting system is shown in Fig. 3. At the center of this system is a 985-μm thick Micron Semiconductor Ltd. type BB1 double-sided Si microstrip detector (DSSD). The DSSD was segmented into 40 one-mm strips in both the x and y dimensions. Two 500-μm thick Si PIN detectors, with active areas 5 cm $\times$ 5 cm, were placed on either side of the DSSD and served as second energy loss detectors for beta particles. An additional 300-μm thick Si PIN detector was placed downstream of the Si PIN – DSSD – Si PIN sandwich and served as a fragment veto detector. The Si detector

stack was mounted on an ISO-160 flange and placed in the beamline under high vacuum. An aluminum degrader foil was placed immediately upstream of the DSSD detector stack. The foil thickness was selected to optimize the implantation of fragments within the first 200 μm of the DSSD. The aluminum degrader thickness was 907 mg/cm^2 for the first A1900 tune and 963 mg/cm^2 for the second tune.

Secondary beam characterization was performed using detectors placed one meter upstream of the DSSD. A parallel plate avalanche counter (PPAC) was used to image the x and y position of the incoming fast beam. The fragment energy loss, for beam particle identification purposes, was measured using a 500 μm Si PIN detector (PIN1). Fragment time-of-flight was determined by the time difference between a particle impinging this Si PIN detector and a radiofrequency pulse from the K1200 cyclotron. Particle identification spectra for the two A1900 tunes are shown in Fig. 4. The secondary beam was defocused to ensure that most of the active area of the DSSD was illuminated. The average implantation rate for all fragments entering the DSSD was 200 Hz for the first A1900 tune and 100 Hz for the second.

One of the challenges of correlating fragment implants with subsequent β decays is the large energy difference between the two types of events. A fragment implant may deposit more than 1 GeV energy into the DSSD, while a β particle deposits less than 1 MeV. Readout of the DSSD strips was accomplished using dual output preamplifiers provided by MultiChannel Systems. The preamplifier circuit provided both high gain (2 V/pC) and low gain (0.1 V/pC) analog output pulses. The output stages could drive 50 Ω inputs to $\pm$2 V. The low gain signals, which provide the fast fragment implantation energy, were sent directly to Phillips 7164H ADCs. The high gain preamplifier signals were further amplified by Pico Systems Shaper/Discriminators in CAMAC. The shaper outputs were digitized by Phillips 7164H ADCs and provided the energy information for β-decay events. The typical energy resolution for a single strip of the DSSD was 90 keV full-width at half maximum measured for the 6.2 MeV α transition from the decay of ^{228}Th. The discriminator outputs from the Pico Systems Shaper/Discriminator were combined in a logical OR gate to provide the master trigger. Individual discriminator signals were also sent to coincidence registers for zero suppressed readout of the DSSD energy ADCs, and to scalers for rate monitoring. Data were written, event-by-event, directly to disk. Each recorded event was tagged with an absolute time stamp generated by a free-running clock, which produced a pulse every

30.5 μs.

γ-ray detection was accomplished using six Ge detectors from the MSU Segemented Germanium Array [13]. Each detector is composed of an 8 cm long by 7 cm diameter Ge crystal divided into eight 1-cm wide segments along the crystal length and four quadrants on the crystal face. Only the signals from the central contact were processed for this experiment. The Ge detectors were oriented in a circular geometry around the DSSD, with the long side of the crystals parallel to the secondary beam axis. This arrangement is shown in Fig. 5. The minimum distance from the center of a Ge cryostat to the center of the DSSD was 12.4 cm. The thickness of the Al vacuum wall positioned between the Ge detectors and the DSSD was 3 mm. A large volume Ge detector was also placed immediately downstream of the β counting system. Two identical outputs were obtained from each Ge preamplifier to get both timing and energy information for each detected event. The energy signals were processed by Ortec 572 shaping amplifiers and digitized using Ortec AD413 8K ADCs. The timing signals passed through Ortec 472 Timing Filter Amplifiers and Tennelec TC455 Constant Fraction Discriminators (CFD). The CFD outputs were used as stop signals to generate digitized β-γ timing curves using a Phillips 7186 TDC, where the common start signal was the master trigger from the DSSD.

A ^{207}Bi source was used to set the DSSD master gate trigger delay for the Ge ADCs. This source has a highly-converted 1063-keV transition in coincidence with a 569-keV γ-ray. The e-γ prompt coincidence was used to establish the time delays for properly gating delayed γ-ray coincidences. The efficiency of the Ge array between 80 keV and 2.6 MeV was experimentally measured for a point source geometry using a NIST Standard Reference Material 4275-C69 source containing ^{125}Sb and ^{154,155}Eu, and a calibrated ^{228}Th source. To account for the extended nature of the fragment implantation pattern in the DSSD, a simulation of the extended source geometry was performed using the Monte Carlo N-Particle (MCNP) code [14]. The calculated peak efficiency of the Ge array for a 1 MeV photon in this geometry was 3.3%. The Ge detectors were energy calibrated between 0.08 and 2.6 MeV using the well-known transitions in ^{154,155}Eu, ^{60}Co, and ^{228}Th.

Fragment-β correlations were established in software by first requiring a high-energy implant event in pixel x, y, where x is a horizontal strip and y a vertical strip of the DSSD. A valid implant was one that produced a signal above threshold in PIN1 and PIN2, as well as a high-energy signal (greater than 10 MeV) in a single strip on both the back and front of the

DSSD (see Fig. 3). The particle identification data (energy loss in PIN1 and time-of-flight), as well as the absolute time stamp, were stored in arrays indexed by x, y. A subsequent β-decay event in the same pixel was one that produced a low-energy signal (less than 5 MeV) above threshold in a single strip on both the back and front of the DSSD and no signal in PIN1. A fragment-β correlated particle identification spectrum (see Fig. 4) was generated using the previously stored particle identification data for the implant event. The differences between the time stamps of β events and correlated implant events were also histogrammed to generate a decay curve. The decay properties for a specific isotope were obtained by selecting the appropriate gate in the correlated particle identification spectrum. To reduce the chances for random correlations, a maximum time of ten seconds was established for any fragment-β correlation. Also, back-to-back implantations in a given pixel that occurred within ten seconds of each other were rejected.

A fragment-β correlation efficiency of 30% was measured for the 2.15×10^6 implant events registered in the DSSD during the first A1900 tune. The correlation efficiency was 40% for the second A1900 tune, where a total of 5.12×10^5 implants were registered in the DSSD. The increased correlation efficiency is attributed to the lower average implant rate associated with the second tune.

RESULTS

^{56}V

A part of the β-delayed γ-ray spectrum for ^{56}V is shown in Fig. 6. The spectrum in Fig. 6(a) represents β-γ events that occurred within one second of a ^{56}V implant. A comparison of this spectrum with one representing β-γ events occurring between four and five seconds (Fig. 6(b)) after a ^{56}V implant was used to distinguish between short- and long-lived β activities. Four transitions have been assigned to the β decay of ^{56}V, and are listed in Table I. The two intense transitions at 668 and 1006 keV are most likely the transitions observed at 700 ± 50 keV and 1000 ± 50 keV by Sorlin *et al.* [10]. A third transition at 340 ± 50 keV, assigned to the decay of ^{56}V in Ref. [10], was not observed in this work. The low-energy transition at 268-keV is a γ ray assigned to ^{57}V decay (see next section). Its appearance in Fig. 6(a) is attributed to the overlap of ^{57}V and ^{56}V in the particle identification spectrum

shown in Fig. 4(b).

The decay curve derived from ^{56}V-correlated β decays is shown in Fig. 7(a). The curve was fitted with a single exponential decay with an exponential background component. The activity of the daughter ^{56}Cr decay, which has $T_{1/2} = 5.9$ min, was not considered. The decay constant for the exponential background was deduced to be 0.144 s^{-1} by fitting the half-life curves for all nuclides implanted along with ^{56}V for the first A1900 tune (see Fig. 4). The identical procedure was used to deduce an exponential decay constant of 0.0815 s^{-1} for the decay curves of nuclides implanted during the second A1900 tune. The fitted half-life curves obtained for ^{57}V, which was produced at both rigidity settings, were used to verify the above treatment of the exponential background.

Decay curves were also obtained from β-γ coincidence data. The decay curve for β particles in coincidence with 1006-keV γ rays is shown in Fig. 7(b). The extracted half-lives $T_{1/2}^{\beta} = 216 \pm 4$ ms and $T_{1/2}^{\beta-1006} = 221 \pm 18$ ms agree with each other and with the previous ^{56}V half-life measurements of 230 ± 25 ms [10] and 240 ± 40 ms [11]. We have adopted the value $T_{1/2} = 216 \pm 4$ ms for ^{56}V.

The proposed decay scheme for levels in ^{56}Cr populated following the β decay of ^{56}V is shown in Fig. 8. The β-decay Q value was derived from the measured mass excess for both parent and daughter as compiled in Ref. [15]. Absolute γ-ray intensities were deduced from the number of observed ^{56}V γ rays, the γ-ray efficiency curve calculated using MCNP, and the number of ^{56}V implants correlated with β decays. The last term was derived from the fit of the decay curve in Fig. 7(a). Placement of the 668-keV γ ray feeding the first excited state at 1006 keV was confirmed by γ-γ coincidences (see Fig. 9). Placement of the 824- and 1318-keV transitions follows the proposed level scheme of Nathan *et al.* [16], who used the ^{11}B + ^{48}Ca fusion evaporation reaction to populate excited states in ^{56}V. β feedings to levels in ^{56}Cr were deduced from the absolute γ-ray intensities, and are summarized in Table II. The log$f$ values were interpolated using the tabulation in Ref. [17]. The predominant β-decay branch is to the 0^+ ground state of ^{56}Cr. The logft value of 4.62 suggests an allowed transition, and we have assigned spin and parity 1^+ to the ground state of the ^{56}V parent. This assignment is consistent with that adopted by Sorlin *et al.* [10]. The 2^+ spin-parity assignments for the 1006, 1830, and 2324 keV states are taken from Refs. [16, 18]. The β branching to the 1674-keV state has a logft value comparable to the feeding to the ground state. We have tentatively assigned 0^+ spin-parity to this state.

^{57}V

A part of the β-delayed γ-ray spectrum for ^{57}V is shown in Fig. 10. This spectrum represents β-γ events that occurred within the first second after a ^{57}V implant. Eight transitions have been assigned to the β decay of ^{57}V, and are listed in Table III. The three transitions at 268, 692, and 942 keV are most likely the 267 ± 4, 700 ± 50, and 900 ± 50 keV γ rays identified by Sorlin *et al.* [10]. The five new γ-ray transitions identified following the decay of ^{57}V have absolute intensities below 5%.

The decay curve derived from ^{57}V-correlated β decays is shown in Fig. 11(a). The curve was fitted with a single exponential decay with an exponential background component. The activity of the daughter ^{57}Cr decay, which has $T_{1/2} = 21$ s, was found not to contribute significantly to the observed β singles activity. Decay curves were also obtained from β-γ coincidence data. The decay curve for β particles in coincidence with the 268- and 692-keV γ rays are shown in Fig. 11(b) and Fig. 11(c), respectively. We have adopted the value $T_{1/2} = 350 \pm 10$ ms for ^{57}V. This value is consistent with the previously measured values of 323 ± 30 ms [10] and 340 ± 80 ms [11].

The proposed decay scheme for levels in ^{57}Cr populated following the β decay of ^{57}V is shown in Fig. 12. The β-decay Q value was derived from the measured mass excess for both parent and daughter as compiled in Ref. [15]. No previous information on excited levels in ^{57}Cr was available in the literature. Based on the coincidence efficiency of the seven-detector germanium array, we should have observed events in our γ-γ matrix if any two of the three most intense γ rays in ^{57}Cr were coincident. No events were recorded above background in the ^{57}V-correlated β-γ-γ matrix. Therefore, the 268-, 692-, and 942-keV γ rays have been placed directly feeding the ground state of ^{57}Cr. The remaining γ-ray transitions were placed based on energy-sum relationships. β feeding to levels in ^{57}Cr was deduced from the absolute γ-ray intensities and is summarized in Table IV. The $\log ft$ values to all states in ^{57}Cr suggest allowed transitions. The spin-parity of the ground state of the parent ^{57}V is proposed to be $7/2^-$ based on systematics. The spin-parity of the ^{57}Cr ground state has been proposed to be $3/2^-$ by Davids *et al.* [19] based on β decay feeding patterns to excited states in ^{57}Mn. This conforms to the spin-parity assignments for the ground states of other neutron-rich, $N = 33$ isotones. A $3/2^-$ spin-parity for the ground state of ^{57}Cr would exclude $7/2$ spin for the ground state of ^{57}V, given our observed β branch to the ground state of

^{57}Cr. Sorlin *et al.* [10] proposed $3/2^-$ spin-parity for the ground state of ^{57}V based on the characteristics of the β decay.

^{58}V

A part of the β-delayed γ-spectrum for ^{58}V is shown in Fig. 13. This spectrum represents β-γ events that occurred within the first second of a ^{58}V implant. Six transitions have been assigned to the β decay of ^{58}V, and are listed in Table V. The 880-keV transition was assigned to ^{58}V decay from our earlier fragmentation study [4]. Sorlin *et al.* observed a broad peak at 900 ± 100 keV in their delayed γ-ray spectrum for ^{58}V [10]. They suggested the presence of two unresolved transitions with approximate energies 800 and 1000 keV. The two γ rays observed at 1041 and 1056 keV in this work may correspond to the higher-energy portion of the unresolved peak at 900 ± 100 keV observed by Sorlin *et al.*, however, the summed intensity of these two transitions is only half that observed for the 880 keV transition. Absence of the 1056-keV transition in the ^{58}V β-delayed γ-ray spectrum in Ref. [4] is attributed to the higher background encountered in that first experiment. The peak height of the 1056-keV γ ray, based on the absolute intensities measured in this work, would have been 15 counts in the γ-ray spectrum presented in Ref. [4]. The appearance of the 268-keV γ ray assigned to ^{57}V decay is attributed to the overlap of ^{57}V and ^{58}V in the particle identification spectrum shown in Fig. 4(d).

The decay curve derived from ^{58}V-correlated β decays is shown in Fig. 14(a). The curve was fitted with a single exponential decay with an exponential background component. A contribution due to the daughter ^{58}Cr decay, which has $T_{1/2} = 7$ s, was investigated but did not contribute significantly to the overall β rate. Decay curves were also obtained from β-γ coincidence data. The decay curve for β particles in coincidence with the 880- and 1056-keV γ rays are shown in Fig. 14(b) and Fig. 14(c), respectively. We have adopted the value $T_{1/2} = 185 \pm 10$ ms for ^{58}V. This value is consistent with our previously measured value of 202 ± 36 ms [4], and those of Sorlin *et al.*, 205 ± 20 ms [10], and Ameil *et al.*, 200 ± 20 ms [11].

The lack of sufficient statistics in the γ-γ matrix for ^{58}V decay makes it difficult to propose a level structure for ^{58}Cr. Based on absolute intensities, the 880-keV γ ray is the most likely candidate for the $2_1^+ \rightarrow 0_1^+$ transition in ^{58}Cr, as proposed in Ref. [7]. From nuclear structure

considerations, the likelihood that the 1056-keV transition is a direct transition to the ground state is small. If the two intense transitions, 880 and 1056 keV, are assumed to be coincident, this would suggest direct β feeding to the ^{58}Cr ground state. An allowed β transition to the ground state of ^{58}Cr would require spin-parity 0^+ or 1^+ for the ^{58}V parent.

DISCUSSION

Potential energy surfaces from Hartree-Fock-Bogoliubov calculations [20] suggest prolate shapes with $\epsilon_2 \approx 0.15$ for $^{56-58}$V [6]. Sorlin *et al.* [10] made a detailed comparison of the measured β-decay properties of ^{56,57,58}V with the results of quasi-particle random-phase approximation (QRPA) calculations. The experimental half-lives and branching ratios were compared with QRPA results where the ground state parent and daughter deformations were systematically changed. The experimental results were best reproduced using $\epsilon_2 =$ 0.167, 0.118, and 0.23 for ^{56}V, ^{57}V, and ^{58}V, respectively. The half-life results reported here do not differ appreciably from those used by Sorlin *et al.* in their QRPA analysis, however, the β branching ratios are very different for ^{56,57}V.

The ground state β branch deduced in this work for the decay of ^{56}V was $70 \pm 2\%$, compared to $55 \pm 10\%$ as reported in Ref. [10]. The larger β branching to the ground state of ^{56}Cr reported here is consistent with a smaller deformation for parent and daughter; Sorlin *et al.* calculated a ^{56}V half-life of 192 ms and a 78% ground state β branch using $\epsilon_2 = 0.1$. These calculated values reproduce well the current findings for the ^{56}V β decay. For ^{57}V, a ground state β branch of $21 \pm 5\%$ has been deduced. This branch is a factor of two smaller than that quoted by Sorlin *et al.* [10]. Based on the QRPA calculations in Ref. [10], a smaller branching ratio may be indicative of a larger ground state deformation for ^{57}Cr and ^{57}V.

We have compared our new experimental data to the results of a number of shell model calculations. The first step in this process was to identify the pf-shell interaction most appropriate for these neutron-rich nuclides. The results of pf-shell model calculations for the low-energy levels in ^{56}Cr and ^{58}Cr using the interactions FPD6 [21], KB3G [22], and GXPF1 and GXPF2 [23] are shown in Fig. 15. The levels were calculated in full pf-model space by the code MSHELL [24]. The GXPF interaction, specifically GXPF1, provides the best description of the peak in the systematic variation of $E(2_1^+)$ at ^{56}Cr, which is indicative

of a substantial subshell closure at $N = 32$. In addition to reproducing the $N = 32$ subshell gap, the shell model results using GXPF1 interaction show a significant gap in the effective single-particle energies determined for the $p_{1/2}$ and $f_{5/2}$ neutron orbits [23]. This $N = 34$ shell gap is predicted to arise only for $_{20}$Ca and $_{22}$Ti isotopes. The low energy of the 2_1^+ state in ^{58}Cr shows the non-existence of the $N = 34$ magic gap for the Cr isotopic chain. Because of the successes of GXPF1 stated above, we have used this interaction to calculate the β-decay properties of the odd-odd isotopes ^{56}V and ^{58}V.

The β decay was calculated in proton-neutron formalism in a truncated basis in which the $f_{7/2}$ shell neutrons are filled. The effect of this truncation was tested by comparing it with an exact calculation for the ^{52}Ca to ^{52}Sc β decay (where the basis dimensions are smaller). This comparison showed that the relative β branchings were similar to about the 20% level, while the overall Gamow-Teller strength was smaller by about an average factor of 2 in the full-space result. In addition, the overall Gamow-Teller strength in the full space is reduced by a factor of 1.81 [22] when compared to experiment (in other pf-shell nuclei); this effect can be attributed to correlations beyond the pf shell. The lifetimes quoted from the present calculations are multiplied by a factor of 4 to take into account these two effects.

The calculated spectra for ^{56}V and ^{58}V both show a low-lying multiplet with spins 1^+, 2^+ and 3^+. Based upon the observation of strong (0^+) ground-state feeding, $J^\pi = 1^+$ was assumed for the ground states in both the ^{56}V and ^{58}V β-decay calculations. The results of these shell-model calculations are given in Table VI. The calculated half-life for ^{56}V compares favorably with the half-life adopted here for ^{56}V, $T_{1/2} = 216 \pm 4$ ms. The half-life value predicted for ^{58}V is a factor 1.6 smaller than the experimental value of 185 ± 10 ms.

A significant shift in the β feeding to excited states is expected between ^{56}V and ^{58}V. Experimentally, we observed a $70 \pm 2\%$ ground state β branch for the ^{56}V decay. Although we have not proposed a level scheme for ^{58}Cr, feeding to the ^{58}Cr ground state can be inferred from the absolute γ-ray intensities listed in Table V. The absolute intensity of the proposed $2_1^+ \rightarrow 0_1^+$ transition at 880 keV is $62 \pm 7\%$, therefore, the maximum direct feeding to the ^{58}Cr ground state is $38 \pm 7\%$. This number would be reduced if any one of the observed β-delayed γ rays directly populated the ground state. The ground state branching for the β decay of ^{58}V is roughly a factor of two smaller than that observed in ^{56}V. A reduction in the ground state feeding between ^{56}V and ^{58}V was also observed in Ref. [10]. This trend is reproduced by the shell model results. The direct β feeding to the first excited 0^+ state in

the even-even daughter is calculated to be significant for the β decays of both ^{56}V and ^{58}V. The shell model results listed in Table VI for the ^{56}V β branching show 8% feeding to the 0_2^+ state in ^{56}Cr. This branching was observed to be $26 \pm 2\%$. Feeding of the 0_2^+ state in ^{56}Cr via unobserved γ rays would reduce the experimental β branching to this state. However, with a detection sensitivity for delayed γ rays from ^{56}V of better than 1% absolute intensity, we do not expect this reduction to be greater than the reported error on the experimental branching ratio. Based on absolute intensities deduced for β-delayed γ rays following the decay of ^{58}V, and the results of the shell model calculations for this decay, the 1056-keV transition is a candidate for the $0_2^+ \rightarrow 2_1^+$ transition in ^{58}Cr. This interpretation would put the first excited 0^+ state in ^{58}Cr at an excitation energy of 1936 keV, slightly above the 0_2^+ excitation energy in ^{56}Cr.

Shell-model calculations were also carried out for the β decay of the odd-A ^{57}V using the same GXPF1 interaction. Since no information is available regarding the ground state of ^{57}V, the energy levels of the parent were calculated. The shell model results show a ground state and first excited state with $J^\pi = 7/2^-$ and $5/2^-$, respectively, separated by only 68 keV. Sorlin et al. [10] have suggested $J^\pi = 3/2^-$ for the ground state of ^{57}V based on the characteristics of the β decay. The first $3/2^-$ state is predicted at 520 keV based on the shell model results. The β-decay properties of ^{57}V to levels in ^{57}Cr were calculated assuming ground-state J^π values $3/2^-$, $5/2^-$, and $7/2^-$. The shell model results for the β branching ratios are listed in Table VII. The general features of the β decay for a $5/2^-$ or $7/2^-$ ground state in ^{57}V are very similar. Direct feeding of the ^{57}Cr ground state is predicted to be greater than 50%, and more than 85% of the β feeding directly populates states in ^{57}Cr below 1.5 MeV in excitation energy. The results assuming a $J^\pi = 3/2^-$ ground state for ^{57}V show little β feeding to ground state of ^{57}Cr, and the main feeding is to three levels below 1 MeV with intensities 19% ($3/2_1^-$), 47% ($1/2_1^-$), and 9.5% ($1/2_2^-$). This feeding pattern is similar to that observed experimentally to the levels in ^{57}Cr at 0, 268, and 942 keV, respectively. However, these results do not reproduce the high feeding to a second low-energy state in ^{57}Cr (the level at 692 keV has a deduced β feeding of 20$\pm$3%). The calculated half-lives for the different decays also are similar, with $T_{1/2,calc.}(^{57}\mathrm{V};3/2^-_{\mathrm{g.s.}}) = 620 \pm 110$ ms, $T_{1/2,calc.}(^{57}\mathrm{V};5/2^-_{\mathrm{g.s.}}) = 650 \pm 110$ ms and $T_{1/2,calc.}(^{57}\mathrm{V};7/2^-_{\mathrm{g.s.}}) = 720 \pm 120$ ms. The errors in the calculated half-lives come from the error in the adopted Q value [15]. Each are about a factor of 1.8 larger than the experimental half-live derived here of $T_{1/2} = 350 \pm 10$ ms.

Significant β strength is observed experimentally to the first excited state in ^{57}Cr at 268 keV, which has an undetermined spin-parity. It should be noted that if the ground state of ^{57}Cr is $3/2^-$ as suggested by Sorlin *et al.* [10], then a direct β branch from a $^{57}V_{34}$ parent with $J^\pi = 7/2^-$ would be a second forbidden transition. The ground state spin of the nearby nucleus $^{59}Mn_{34}$ has been determined to be $5/2^-$ [25]. It is difficult to infer more from the experimental data without a firm spin-parity assignment for the ground state of the ^{57}V parent.

SUMMARY

β decay of the neutron-rich ^{56,57,58}V isotopes was used to populate excited states in the daughter ^{56,57,58}Cr nuclides, respectively. The low-energy levels of the even-even ^{56,58}Cr isotopes were compared to full pf-shell model calculations using a number of available pf-shell interactions. The peak in the systematic variation of $E(2_1^+)$ observed at $N = 32$ for the Cr isotopes was best reproduced by the calculations employing the GXPF1 interaction. However, the other interactions (FPD6, K3BG, and GXPF2) yielded better predictions of the excitation energies of the lowest 0^+, 2^+, and 4^+ states in ^{56}Cr.

The β-decay properties of ^{56,57,58}V were also compared to shell model calculations carried out in a truncated model space using the GXPF1 interaction. A summary of the β-decay properties is given in Table VIII. A factor of four correction has been applied to the overall Gamow-Teller strengths to account for the truncation of the pf-model space and correlations beyond the pf shell. With this correction, the results for the ^{56,58}V decays reproduce the experiment fairly well. The more complicated decay of odd-A ^{57}V was not as tractable; the combined experimental and shell model results suggest $J^\pi = 3/2^-$ for the ^{57}Cr ground state and $J^\pi = 3/2^-$ for the ^{57}V ground state. Unfortunately, shell model calculations of the β decay for these nuclides in the full space is not computationally possible. The final word on these results must wait until the full pf-space result with several interactions is available.

The $N = 32$ subshell gap evidenced by the peak in $E(2_1^+)$ in the Cr isotopes is expected to be more significant for the neutron-rich $_{22}$Ti and $_{20}$Ca isotopes, based on results using the GXPF1 interaction. In additon, the effective single-particle energies calculated using GXPF1 show a significant gap between the $\nu p_{1/2}$ and $\nu f_{5/2}$ orbitals, suggesting that $N = 34$ is a new magic number for neutron-rich nuclides. Further experimental and theoretical

studies are warranted to fully appreciate the implications that an $N = 34$ shell closure would have on the β-decay properties of neutron-rich nuclides in this region of the chart of the nuclides.

This work was supported in part by the National Science Foundation Grants PHY-01-10253, PHY-97-24299, and PHY-00-70911. The authors would like to thank the NSCL operations staff for providing the primary and secondary beams for this experiment.

---

[1] A. Huck, G. Klotz, A. Knipper, C. Miehe, C. Richard-Serre, G. Walter, A. Poves, H.L. Ravn, and G. Marguier, Phys. Rev. C**31**, 2226 (1985).

[2] X.L. Tu, X.G. Zhou, D.J. Vieira, J.M. Wouters, Z.Y. Zhou, H.L. Seifert, and V.G. Lind, Z. Phys. A**337**, 361 (1990).

[3] F. Tondeur, CERN Report 81-09, 81 (1981).

[4] J.I. Prisciandaro, P.F. Mantica, B.A. Brown, D.W. Anthony, M.W. Cooper, A. Garcia, D.E. Groh, A. Komives, W. Kumarasiri, P.A. Lofy, A.M. Oros-Peusquens, S.L. Tabor, and M. Wiedeking, Nucl. Phys. **A682**, 200c (2001).

[5] Table of Isotopes, 8th edition, R.B. Firestone, ed., (Wiley, New York, 1996).

[6] O. Sorlin, C. Donzaud, L. Axelsson, M. Belleguic, R. Beraud, C. Borcea, G. Canchel, E. Chabanat, J.M. Daugas, A. Emsallem, D. Guillemaud-Mueller, K.-L. Kratz, S. Leenhardt, M. Lewitowicz, C. Longour, M.J. Lopez, F. de Oliveira Santos, L. Petizon, B. Pfeiffer, F. Pougheon, M.G. Saint-Laurent, and J.E. Sauvestre, Nucl. Phys. **A669**, 351 (2000).

[7] J.I. Prisciandaro, P.F. Mantica, B.A. Brown, D.W. Anthony, M.W. Cooper, A. Garcia, D.E. Groh, A. Komives, W. Kumarasiri, P.A. Lofy, A.M. Oros-Peusquens, S.L. Tabor, and M. Wiedeking, Phys. Lett. B**510**, 17 (2001).

[8] T.W. Burrows, Nucl. Data Sheets **76**, 191 (1995).

[9] M.R. Bhat, Nucl. Data Sheets **85**, 415 (1998).

[10] O. Sorlin, V. Borrel, S. Grévy, D. Guillemaud-Mueller, A.C. Mueller, F. Pougheon, W. Böhmer, K.-L. Kratz, T. Mehren, P. Möller, B. Pfeiffer, T. Rauscher, M.G. Saint-Laurent, R. Anne, M. Lewitowicz, A. Ostrowski, T. Dörfler, and W.D. Schmidtt-Ott, Nucl. Phys. **A632**, 205 (1998).

[11] F. Ameil, M. Bernas, P. Armbruster, S. Czajkowski, Ph. Dessagne, H. Geissel, E. Hanelt,

C. Kozhuharov, C. Miehe, C. Donzaud, A. Grewe, A. Heinz, Z. Janas, M. deJong, W. Schwab, and S. Steinhäuser, Eur. J. Phys. A **1**, 275 (1998).

[12] J.I. Prisciandaro, A.C. Morton, and P.F. Mantica, Nucl. Instrum. Methods in Phys. Res. in press.

[13] W.F. Mueller, J.A. Church, T. Glasmacher, D. Gutknecht, G. Hackman, P.G. Hansen, Z. Hu, K.L. Miller, P. Quirin, Nucl. Instrum. Meth. Phys. Res. A **466**, 492 (2001).

[14] MCNP^{TM}-A General Monte Carlo N-Particle Transport Code, Version 4C, ed. J.F. Briesmeister, LA-13709-M, 2000.

[15] G. Audi and A.H. Wapstra, Nucl. Phys. **A595**, 409 (1995).

[16] A.M. Nathan, J.W. Olness, E.K. Warburton, and J.B. McGrory, Phys. Rev. C**16**, 192 (1977).

[17] N.B. Gove and M.J. Martin, At. Data Nucl. Data Tables **10**, 206 (1971).

[18] T.T. Bardin, J.G. Pronko, R.E. McDonald, A.R. Poletti, and J.B. McGrory, Phys. Rev. C**14**, 1782 (1975).

[19] C.N. Davids, D.F. Geesaman, S.L. Tabor, M.J. Murphy, E.B. Norman, and R.C. Pardo, Phys. Rev. C **17**, 1815 (1978).

[20] M. Girod, Ph. Dessagne, M. Bernas, M. Langevin, F. Pougheon, P. Roussel, Phys. Rev. C **37**, 2600 (1988).

[21] W.A. Richter, M.G. Van der Merwe, R.E. Julies, and B.A. Brown, Nucl. Phys. **A523**, 325 (1991).

[22] A. Poves, J. Sanchez-Solano, E. Caurier and F. Nowacki, Nucl. Phys. A **694**, 157 (2001).

[23] M. Honma, B.A. Brown, T. Mizusaki, and T. Otsuka, Nucl. Phys. **A704** 134 (2002); M. Honma, T. Otsuka, B.A. Brown and T. Mizusaki, Phys. Rev. C **65**, 061301 (2002).

[24] T. Mizusaki, RIKEN Accel. Prog. Rep. **33**, 14 (2000).

[25] M. Oinonen, U. Köster, J. Aysto, V. Fedoseyev, V. Mishin, J. Huikari, A. Jokinen, A. Nieminen, K. Perajarvi, A. Knipper, G. Walter, and the ISOLDE Collaboration, Eur. Phys. J. A **10**, 123 (2001).

FIG. 1: Systematics of the 2_1^+ states in the even-even $_{24}$Cr isotopes. Data are from Refs. [4–6].

FIG. 2: Low-energy level structures of the $N = 29$ isotones $^{49}_{20}$Ca and $^{57}_{28}$Ni. The levels are labelled with their normalized spectroscopic factors (C^2S) as compiled for ^{48}Ca(d,p)^{49}Ca [8] and ^{58}Ni(p,d)^{57}Ni [9].

FIG. 3: Schematic of the Si detector layout for the NSCL β counting system. Dimensions are not to scale. The PPAC and PIN1 were located one meter upstream of the DSSD stack.

FIG. 4: Particle identification spectrum (a) and fragment-β correlated particle identification spectrum (b) for A1900 settings $B\rho_1 = 4.0417$ Tm and $B\rho_2 = 3.7554$ Tm. Spectra (c) and (d) are the same as above, but for $B\rho_1 = 4.1261$ Tm and $B\rho_2 = 3.8417$ Tm.

FIG. 5: Schematic of the Ge array as it was positioned around the β counting station.

FIG. 6: Part of the β-delayed γ-ray spectrum for ^{56}V, showing (a) only events within the first second of a ^{56}V implant; (b) events in the range four to five seconds after a ^{56}V implant.

FIG. 7: Decay curves for ^{56}V, showing (a) fragment-β correlations only, where the data were fitted with a single exponential decay decay with exponential background; and (b) fragment-β correlations with an additional coincidence with the 1006-keV transition in ^{56}V, where the data were fitted with a single exponential with constant background.

FIG. 8: Proposed level scheme for ^{56}Cr populated following the β decay of ^{56}V. The number in brackets following the γ-ray decay energy is the absolute γ intensity. The Q_β value was deduced from data in Ref. [15]. Identified coincidence relationships are shown by the filled circles.

FIG. 9: γ-γ coincidence gates for the (a) 668-keV and (b) 1006-keV transitions following ^{56}V β decay.

FIG. 10: Part of the β-delayed γ-ray spectrum for ^{57}V. A gate was placed on the decay curve to include only events within the first second of a ^{57}V implant.

FIG. 11: Decay curves for ^{57}V showing (a) fragment-β correlations only, where the data were fitted with a single exponential decay with exponential background; (b) fragment-β correlations with an additional requirement of a 268-keV γ-ray; and (c) fragment-β correlations with an additional requirement of a 692-keV γ-ray. The curves shown in (b) and (c) were fitted with a single exponential decay with constant background.

FIG. 12: Proposed level scheme for ^{57}Cr populated following the β decay of ^{57}V. The number in brackets following the γ-ray decay energy is the absolute γ intensity. The Q_β value was deduced from data in Ref. [15].

FIG. 13: Part of the β-delayed γ-ray spectrum for ^{58}V in the energy range (a) 0 to 1400 keV; and (b) 1400 to 2300 keV. A gate was placed on the decay curve to include only events within the first second of a ^{58}V implant.

FIG. 14: Decay curves for ^{58}V showing (a) only fragment-β correlation, where the data were fitted with a single exponential decay with exponential background; (b) fragment-β correlations with an additional requirement of a 880-keV γ ray; and (c) fragment-β correlations with an additional requirement of a 1056-keV γ ray. The curves shown in (b) and (c) were fitted with a single exponential with constant background.

FIG. 15: Results for low-energy levels in ^{56}Cr and ^{58}Cr for a number of full pf-shell model calculations employing different pf-shell interactions: FPD6 – potential model fit hamiltonian [21], KB3G – G-matrix with monopole corrections [22], GXPF1 and GXPF2 – effective two-body matrix elements with some replacement by the G-matrix [23].

TABLE I: γ rays observed following the decay of ^{56}V.

E_γ(keV)	$I_\gamma^{\rm abs}$(%)	Initial State (keV)	Final State (keV)
668.4 ± 0.3	26 ± 2	1674	1006
824.1 ± 0.9	1.0 ± 0.5	1830	1006
1006.1 ± 0.3	30 ± 2	1006	0
1317.9 ± 0.5	1.0 ± 0.5	2324	1006

TABLE II: β intensities and logft values in the ^{56}V decay to bound levels in ^{56}Cr.

E_x(keV)	I_β(%)	logft^a
0	70 ± 2	4.62 ± 0.07
1006.1 ± 0.3	< 4	> 5.63
1674.5 ± 0.4	26 ± 2	4.63 ± 0.11
1830 ± 1	1.0 ± 0.5	6.01 ± 0.50
2324.0 ± 0.6	1.0 ± 0.5	5.87 ± 0.50

[a]Based on $Q_\beta = 9.05 \pm 0.24$ MeV [15] and $T_{1/2} = 216 \pm 4$ ms.

TABLE III: γ rays observed following the decay of ^{57}V.

E_γ(keV)	I_γ^{abs}(%)	Initial State (keV)	Final State (keV)
249.3 ± 0.7	2 ± 1	942	693
267.8 ± 0.3	52 ± 4	268	0
425.3 ± 0.5	3 ± 1	693	268
692.4 ± 0.4	20 ± 3	693	0
892.5 ± 0.6	1.0 ± 0.5	1583	942
941.7 ± 0.5	7 ± 1	942	0
1289.6 ± 0.5	2 ± 1		
1314.3 ± 0.5	2 ± 1	1583	268

TABLE IV: β intensities and logft values in the ^{57}V decay to bound levels in ^{57}Cr.

E_x(keV)	I_β(%)	logft^a
0	21 ± 5	5.09 ± 0.17
267.8 ± 0.3	47 ± 7	4.67 ± 0.12
692.7 ± 0.4	20 ± 3	4.93 ± 0.21
941.9 ± 0.3	9 ± 2	5.20 ± 0.27
1583 ± 1	3 ± 2	5.51 ± 0.68

[a]Based on $Q_\beta = 8.0 \pm 0.3$ MeV [15] and $T_{1/2} = 350 \pm 10$ ms.

TABLE V: γ rays observed following the decay of ^{58}V.

E_γ(keV)	I_γ^{abs}(%)	Initial State (keV)	Final State (keV)
879.7 ± 0.4	62 ± 7	880	0
1041.2 ± 0.7	8 ± 3		
1056.4 ± 0.5	28 ± 4		
1501.4 ± 0.6	5 ± 2		
1570.6 ± 0.6	5 ± 2		
2216.8 ± 0.7	13 ± 2		

TABLE VI: Comparison of shell model results for the β decay of odd-odd ^{56}V and ^{58}V. The calculations were performed using the GXPF1 interaction [23].

	^{56}V			^{58}V		
J^π final	E_β (MeV)	Branch (%)	log ft	E_β (MeV)	Branch (%)	log ft
0_1^+	9.1	81.2	4.02	12.0	44.8	4.50
2_1^+	8.0	5.3	4.94	11.0	0.4	6.37
2_2^+	6.9	2.2	5.04	9.8	0.8	5.80
0_2^+	6.7	8.5	4.40	9.7	34.3	4.16
0_3^+	5.0	0.4	5.20	9.3	8.3	4.70
$T_{1/2}$[a]		250 ± 25 ms			110 ± 20 ms	

[a]The error in the theoretical number comes from the error in the reported Q value.

TABLE VII: Comparison of shell model results for the β decay of odd-even ^{57}V to levels in ^{57}Cr. The calculated energy levels for ^{57}V suggest a doublet of states with $J^\pi = 5/2^-$ and $J^\pi = 7/2^-$ with an energy difference of 68 keV at the ground state. Sorlin et al. [10] also have suggested $J^\pi = 3/2^-$ for the ^{57}V ground state based on the characteristics of the β decay. The β decay branchings to states in ^{57}Cr have therefore been calculated using the GXPF1 interaction considering each potential ^{57}V ground state spin.

		$J^\pi_{\text{g.s.}} = 3/2^-$		$J^\pi_{\text{g.s.}} = 5/2^-$		$J^\pi_{\text{g.s.}} = 7/2^-$	
E_f	J^π_f	BR(%)	log ft	BR(%)	log ft	BR(%)	log ft
0	$5/2^-$	4.0	5.48	52.9	4.38	69.0	4.31
156	$3/2^-$	19.0	4.76	0.7	6.19		
190	$1/2^-$	47.0	4.36				
707	$5/2^-$	3.0	5.41	9.1	4.95	1.6	5.74
778	$3/2^-$	6.3	5.08	22.5	4.54		
792	$1/2^-$	9.5	4.89				
1066	$7/2^-$			0.4	6.23	5.4	5.13
1135	$9/2^-$					4.4	5.19
1265	$7/2^-$			4.5	5.10	1.9	5.51
1397	$5/2^-$	0.7	5.86	0.2	6.37	1.7	5.52
1415	$3/2^-$			0.3	6.31		
1482	$9/2^-$					1.8	5.48
Sum		89.4		90.6		85.8	

TABLE VIII: Summary of β decay properties derived in this work compared to shell model results using the GXPF1 interaction.

			$T_{1/2}$(ms)				Ground state β branch (%)		
Isotope	$J^{\pi}_{\text{g.s.}}$	$Q_{\beta}(MeV)^{a}$	Theory^{b}	This Work	Ref. [11]	Ref. [10]	Theory	This Work	Ref. [10]
^{56}V	1^{+}	9.05 ± 0.24	250 ± 25	216 ± 4	240 ± 40	230 ± 25	81	70 ± 2	55 ± 10
^{57}V	$3/2^{-}$	8.0 ± 0.3	620 ± 110	350 ± 10	340 ± 80	323 ± 30	4	21 ± 5	55 ± 5
	$5/2^{-}$		650 ± 110				53		
	$7/2^{-}$		720 ± 120				69		
^{58}V	1^{+}	12.0 ± 0.3	110 ± 20	185 ± 10	200 ± 20	205 ± 20	45	< 45	20 ± 10

[a] Taken from Ref. [15].

[b] The error in the theoretical number comes from the error in the reported Q value.

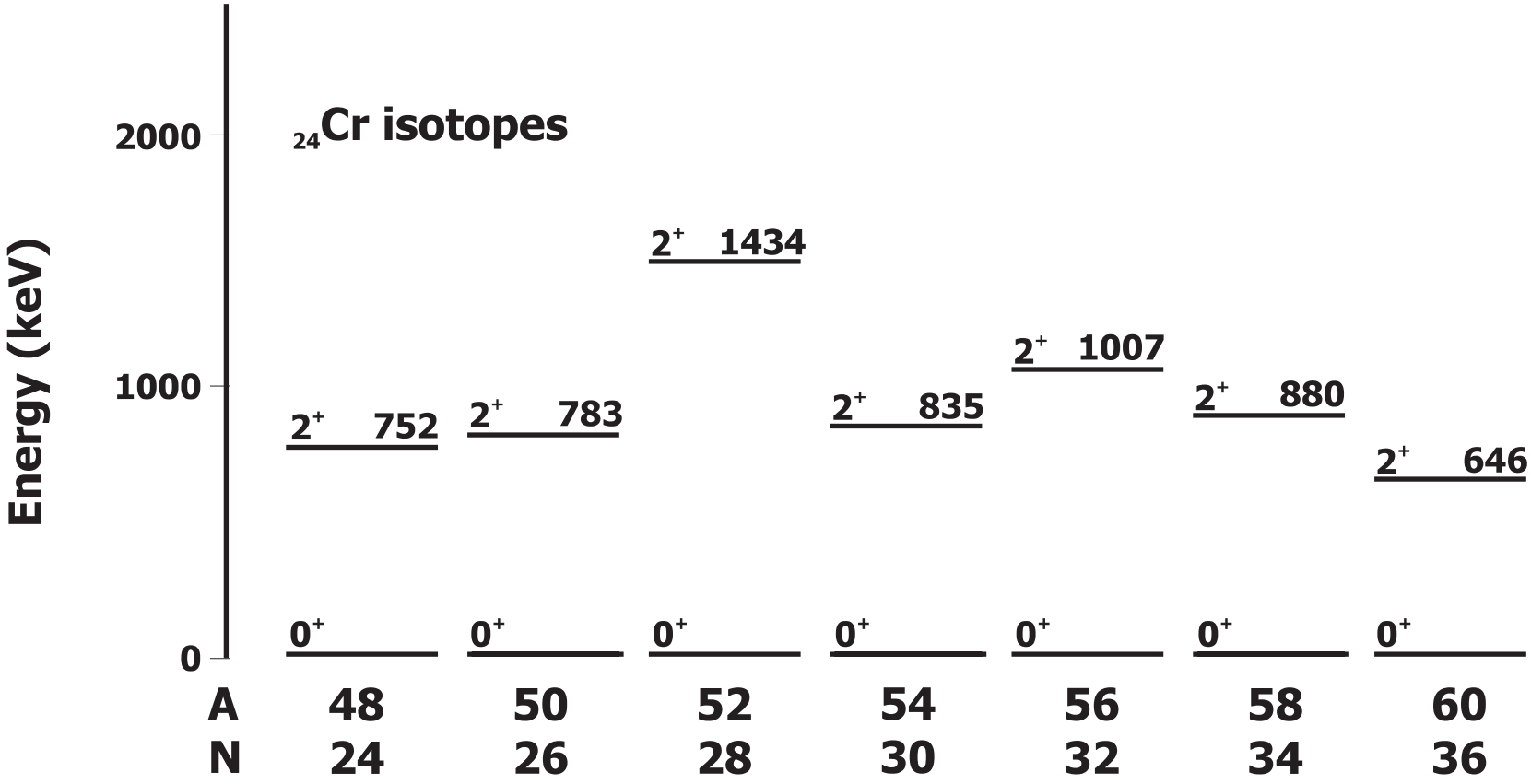
Energy (keV)
2000
1000
0
$_{24}$Cr isotopes
2^+ 752
2^+ 783
2^+ 1434
2^+ 835
2^+ 1007
2^+ 880
2^+ 646
0^+
0^+
0^+
0^+
0^+
0^+
0^+
A 48 50 52 54 56 58 60
N 24 26 28 30 32 34 36

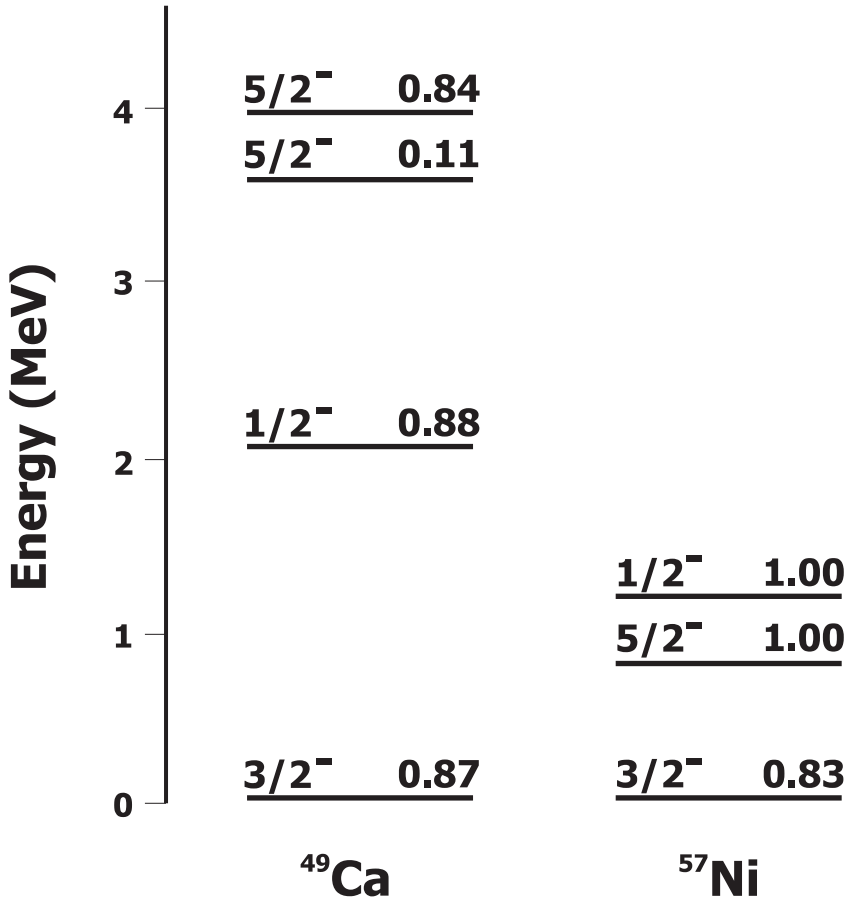
Energy (MeV)
4
3
2
1
0
5/2⁻ 0.84
5/2⁻ 0.11
1/2⁻ 0.88
3/2⁻ 0.87
1/2⁻ 1.00
5/2⁻ 1.00
3/2⁻ 0.83
49Ca
57Ni

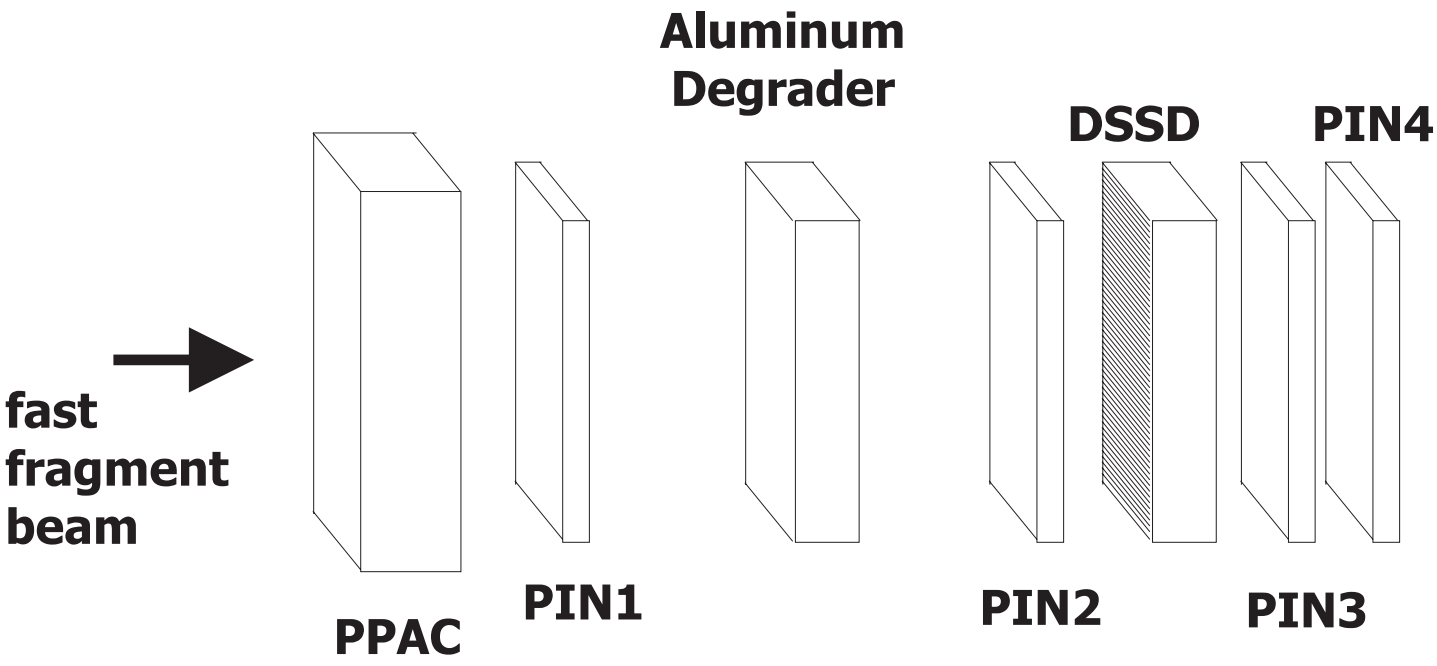
Aluminum
Degrader
DSSD
PIN4
fast
fragment
beam
PPAC
PIN1
PIN2
PIN3

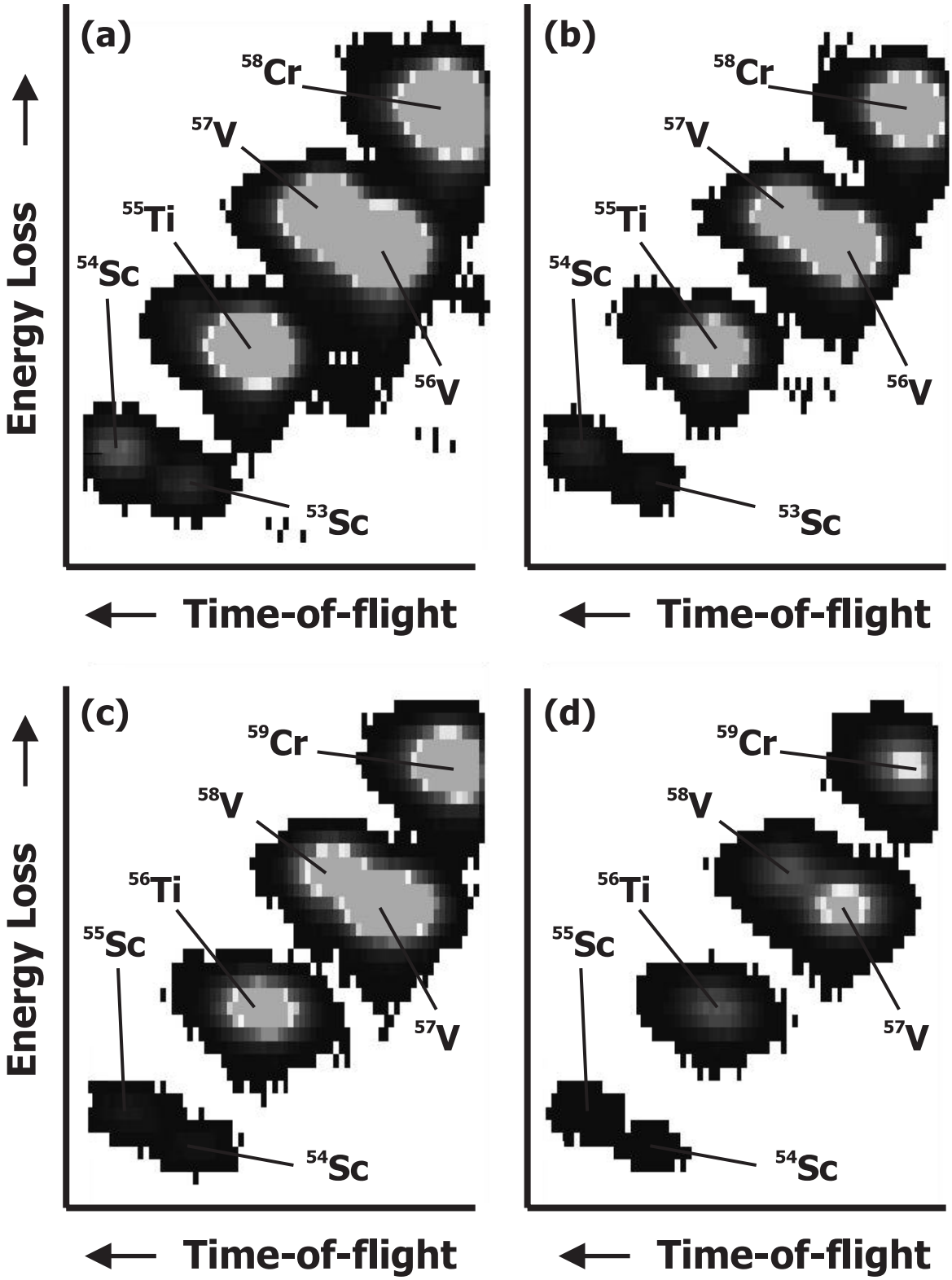
(a)
^{58}Cr
^{57}V
^{55}Ti
^{54}Sc
^{56}V
^{53}Sc
Energy Loss
Time-of-flight
(b)
^{58}Cr
^{57}V
^{55}Ti
^{54}Sc
^{56}V
^{53}Sc
Time-of-flight
(c)
^{59}Cr
^{58}V
^{56}Ti
^{55}Sc
^{57}V
^{54}Sc
Energy Loss
Time-of-flight
(d)
^{59}Cr
^{58}V
^{56}Ti
^{55}Sc
^{57}V
^{54}Sc
Time-of-flight

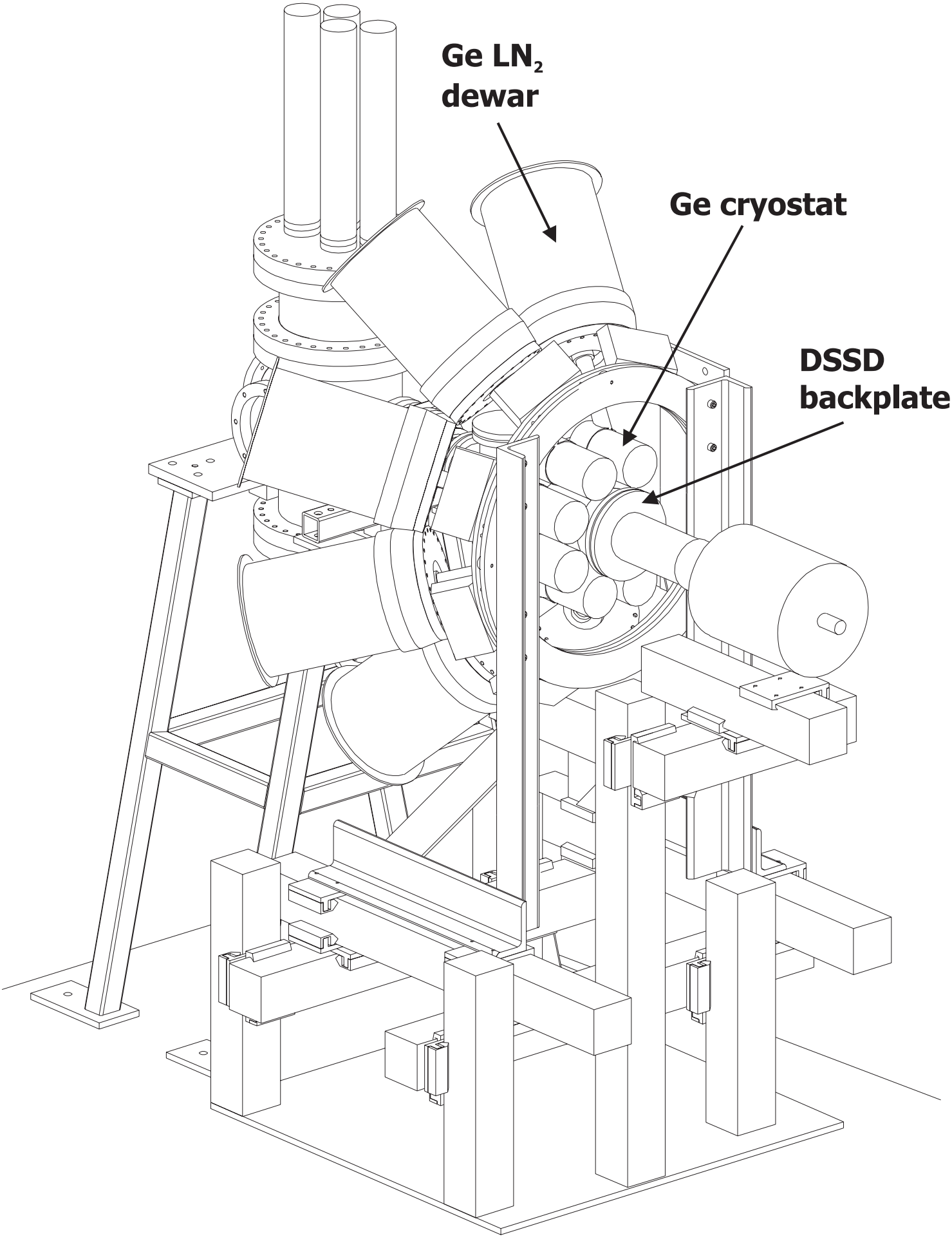
Ge LN2
dewar
Ge cryostat
DSSD
backplate

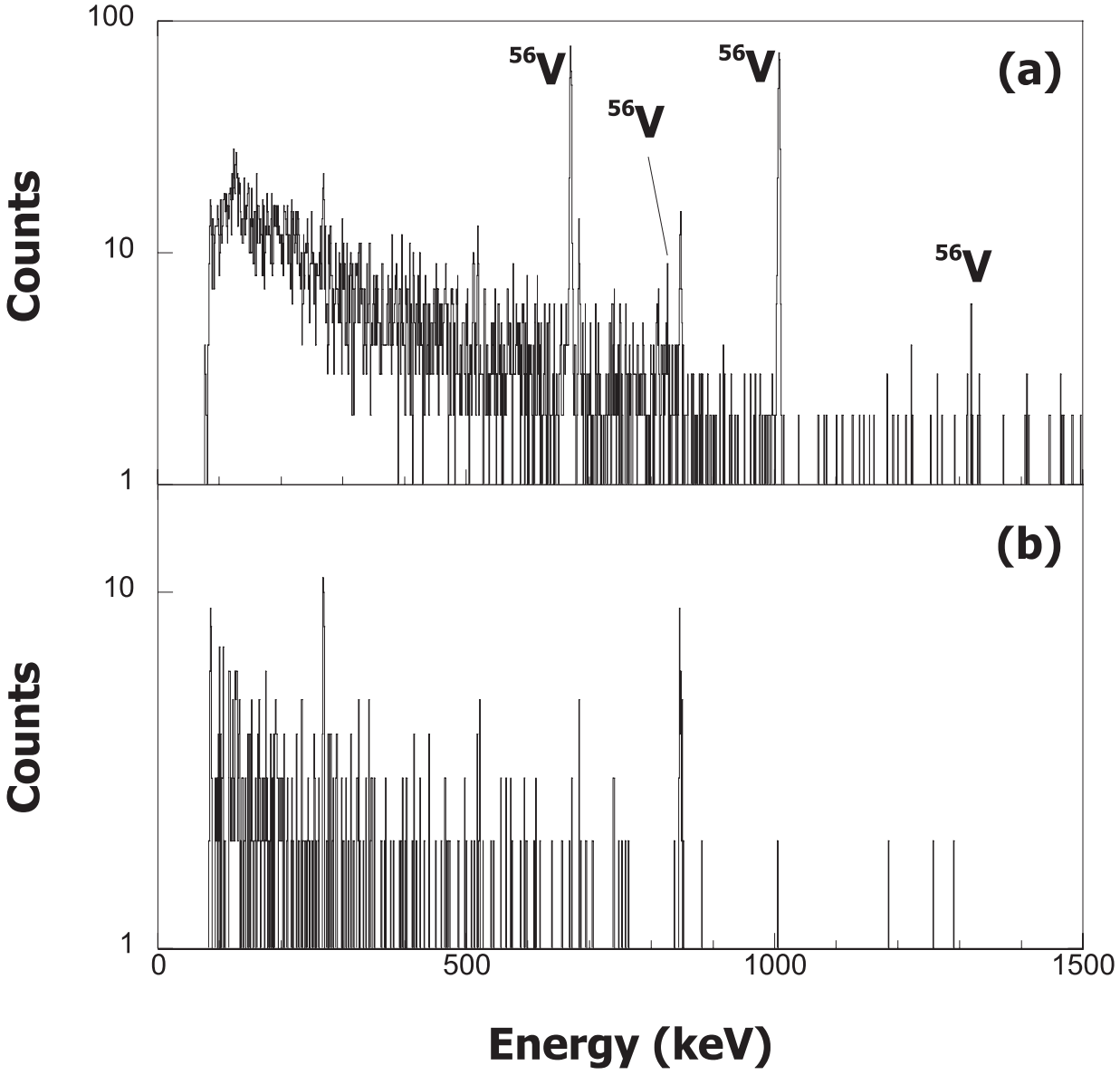
100
10
1
Counts
^{56}V
^{56}V
^{56}V
^{56}V
(a)
(b)
10
1
Counts
0
500
1000
1500
Energy (keV)

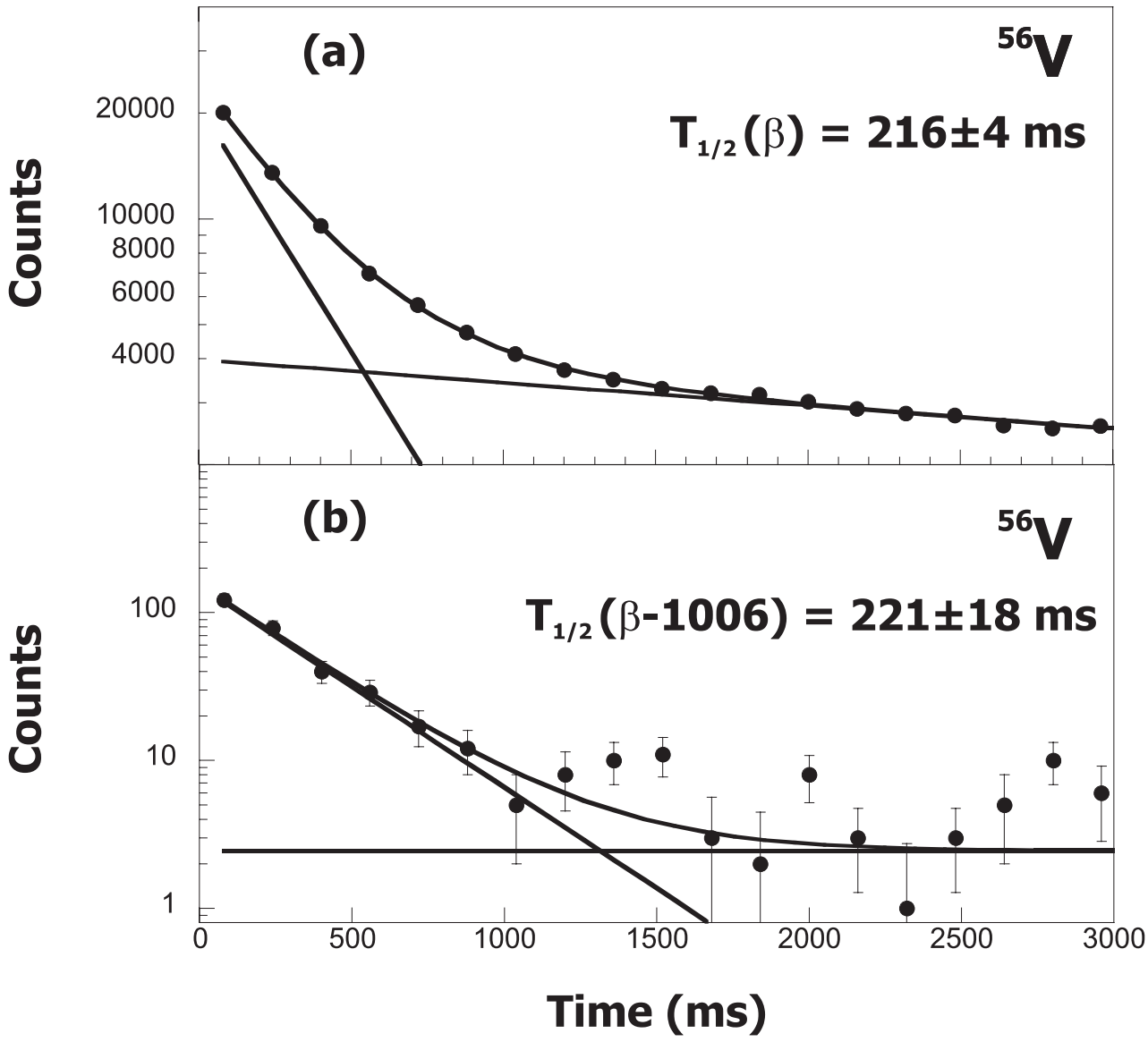
(a)
^{56}V
$T_{1/2}(\beta) = 216\pm4$ ms
Counts
20000
10000
8000
6000
4000
(b)
^{56}V
$T_{1/2}(\beta\text{-}1006) = 221\pm18$ ms
Counts
100
10
1
0
500
1000
1500
2000
2500
3000
Time (ms)

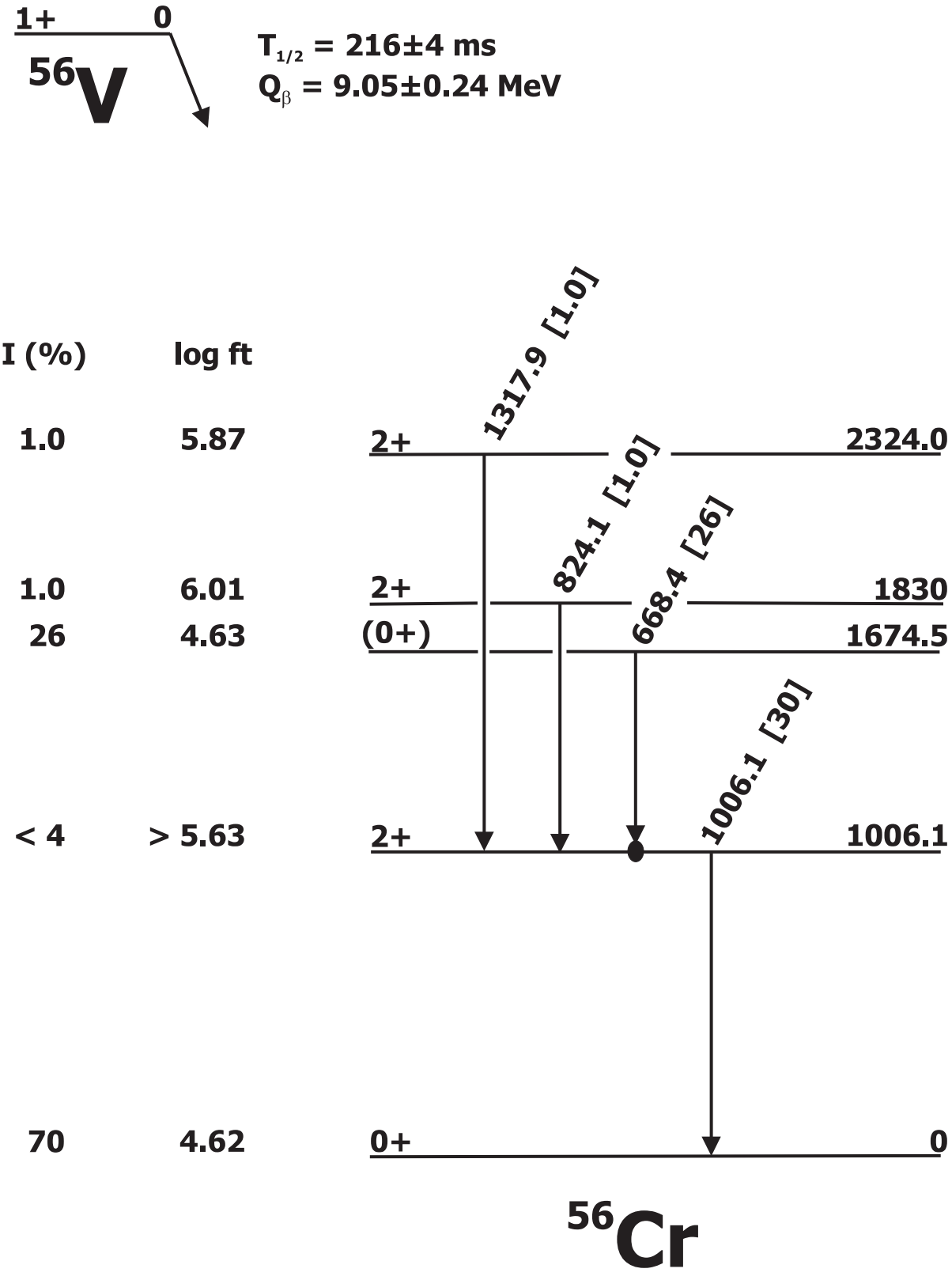
1+
0
56V
T1/2 = 216±4 ms
Qβ = 9.05±0.24 MeV
I (%)
log ft
1.0
5.87
2+
2324.0
1317.9 [1.0]
1.0
6.01
2+
1830
824.1 [1.0]
26
4.63
(0+)
1674.5
668.4 [26]
< 4
> 5.63
2+
1006.1
1006.1 [30]
70
4.62
0+
0
56Cr

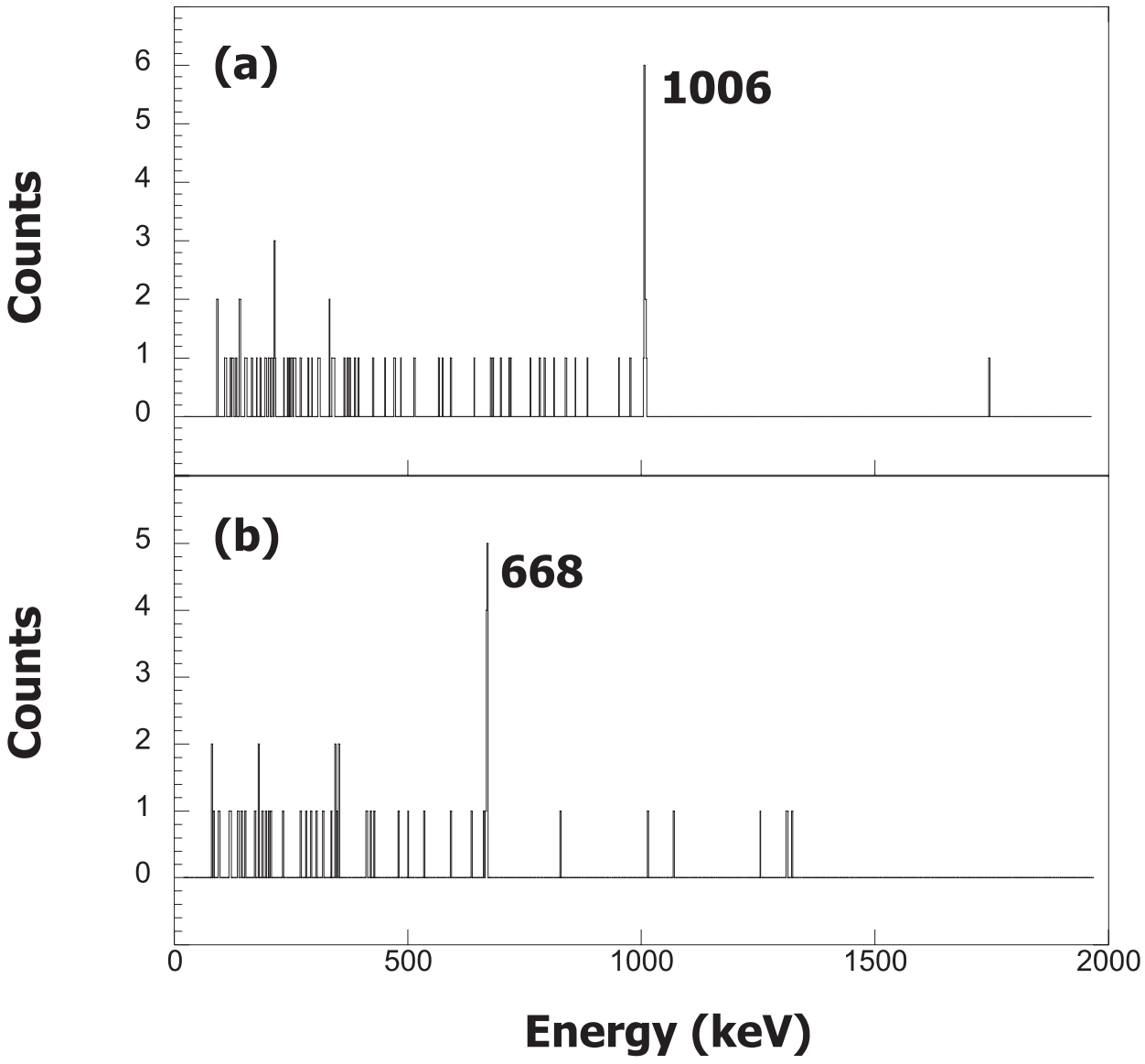
(a)
1006
Counts
6
5
4
3
2
1
0
(b)
668
Counts
5
4
3
2
1
0
0
500
1000
1500
2000
Energy (keV)

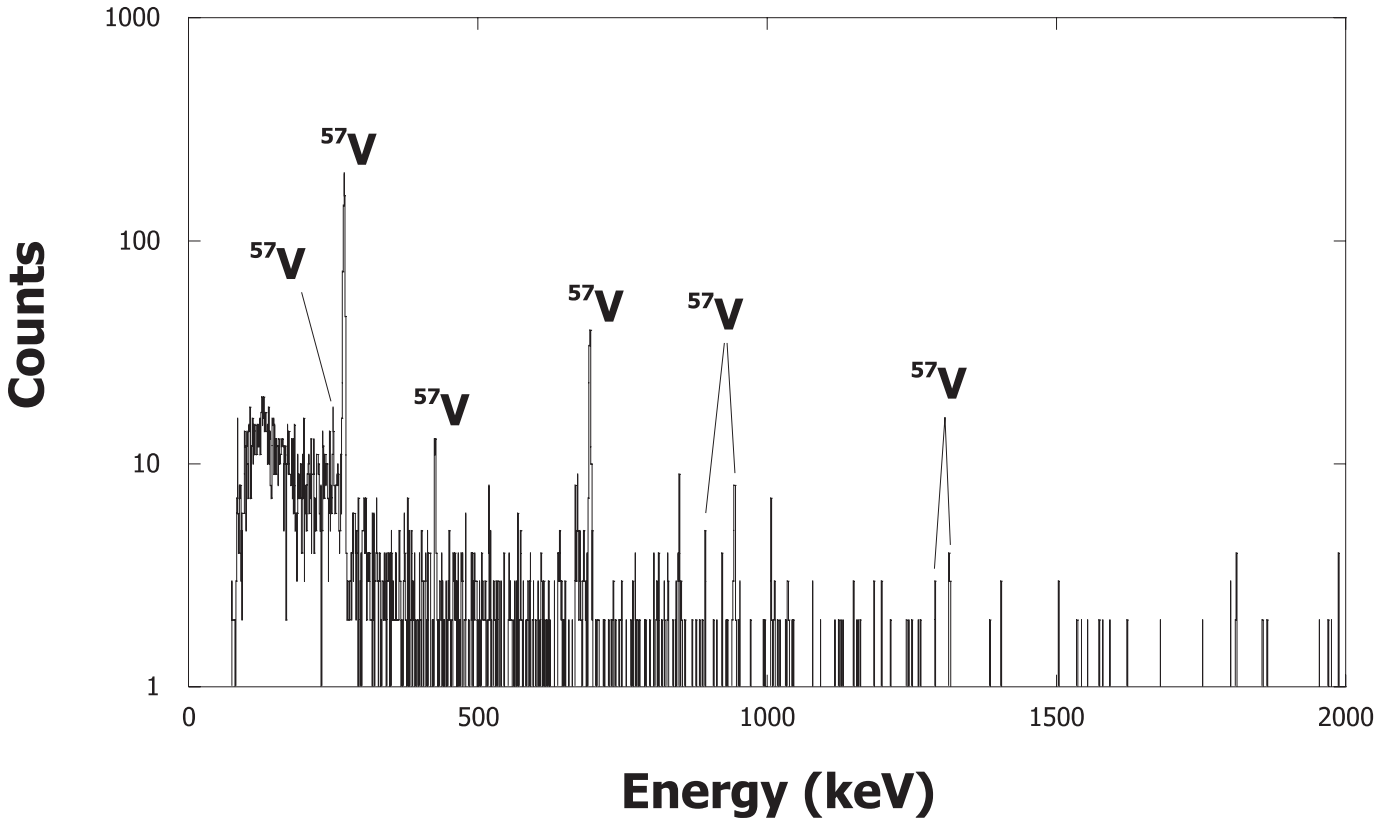
1000
100
10
1
Counts
0
500
1000
1500
2000
Energy (keV)
57V
57V
57V
57V
57V

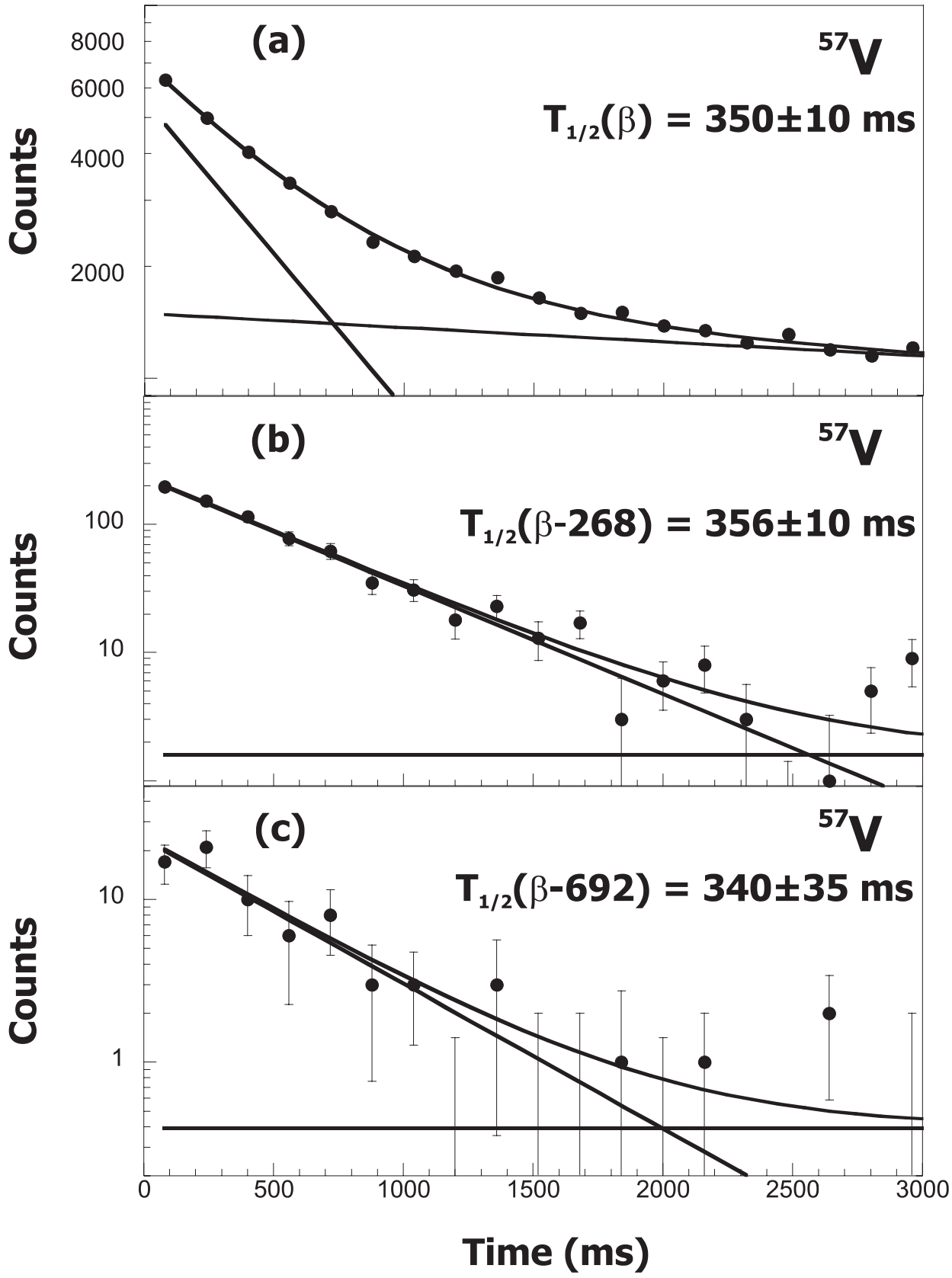
(a)
^{57}V
$T_{1/2}(\beta)$ = 350±10 ms
(b)
^{57}V
$T_{1/2}(\beta\text{-}268)$ = 356±10 ms
(c)
^{57}V
$T_{1/2}(\beta\text{-}692)$ = 340±35 ms
Counts
Counts
Counts
8000
6000
4000
2000
100
10
10
1
0
500
1000
1500
2000
2500
3000
Time (ms)

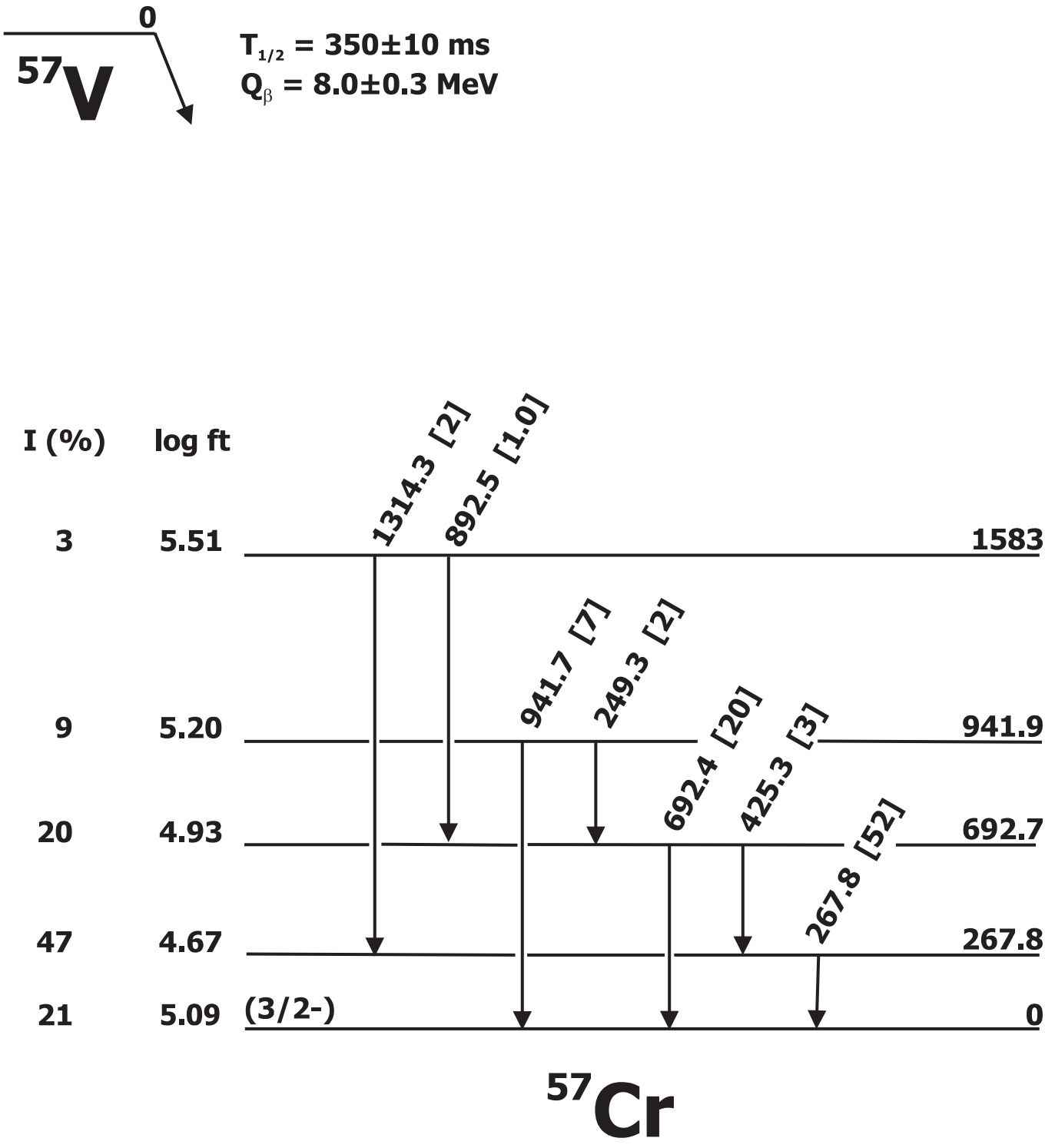
0
57V
T1/2 = 350±10 ms
Qβ = 8.0±0.3 MeV
I (%)
log ft
1314.3 [2]
892.5 [1.0]
3
5.51
1583
941.7 [7]
249.3 [2]
9
5.20
941.9
692.4 [20]
425.3 [3]
20
4.93
692.7
267.8 [52]
47
4.67
267.8
21
5.09
(3/2-)
0
57Cr

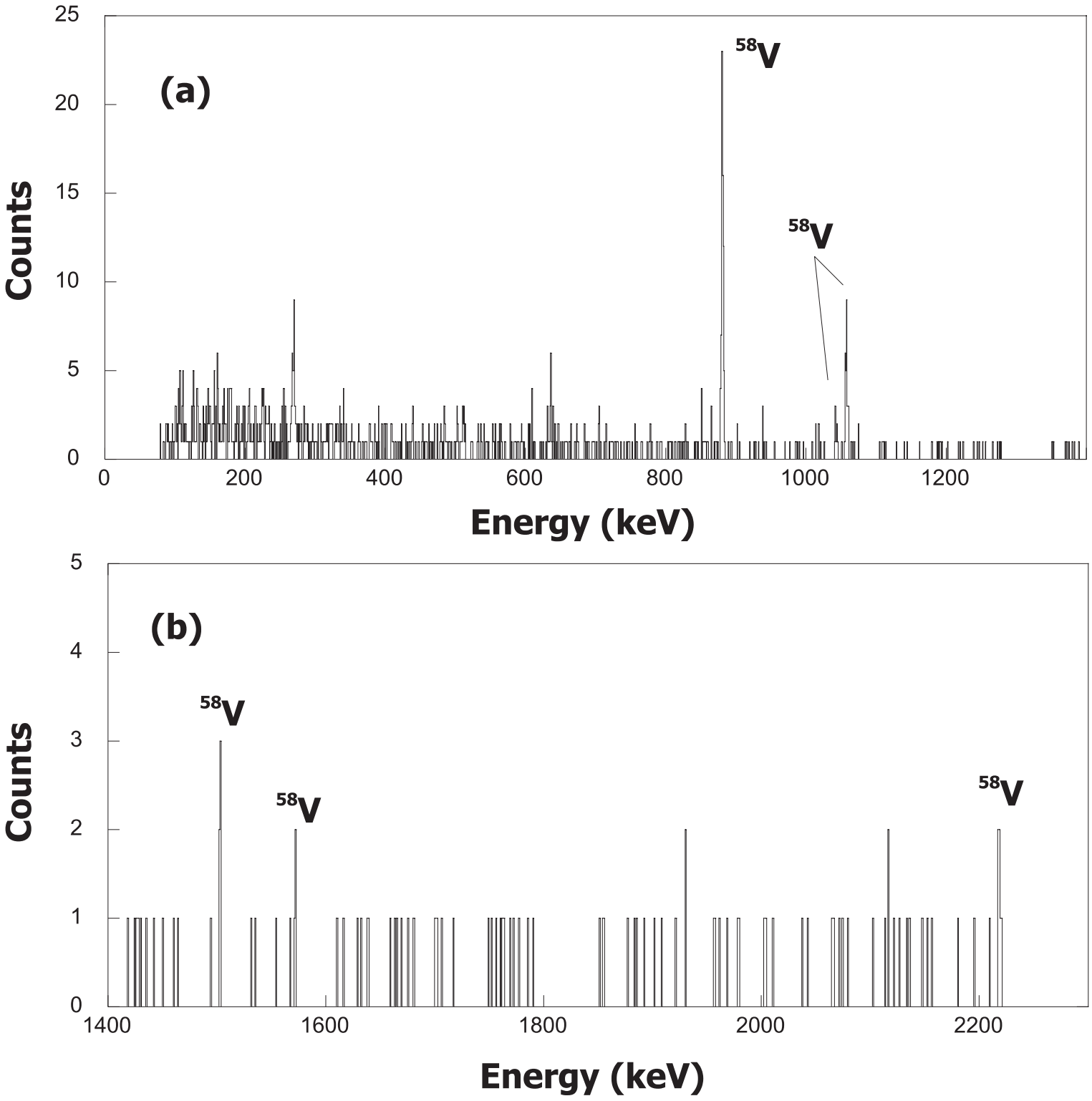
(a)
^{58}V
^{58}V
Counts
Energy (keV)
0
5
10
15
20
25
0
200
400
600
800
1000
1200
(b)
^{58}V
^{58}V
^{58}V
Counts
Energy (keV)
0
1
2
3
4
5
1400
1600
1800
2000
2200

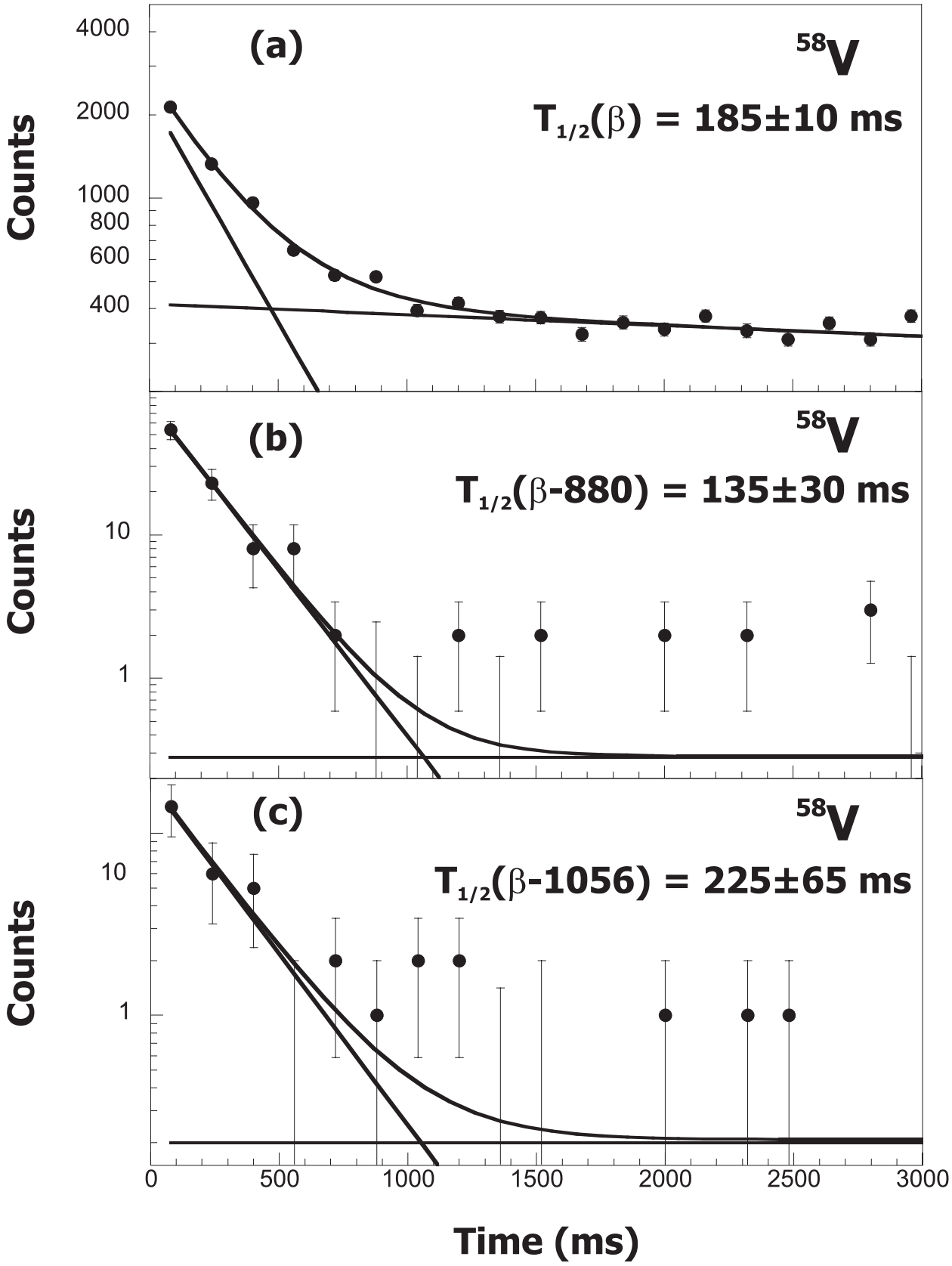
(a)
^{58}V
$T_{1/2}(\beta) = 185\pm10$ ms
(b)
^{58}V
$T_{1/2}(\beta\text{-}880) = 135\pm30$ ms
(c)
^{58}V
$T_{1/2}(\beta\text{-}1056) = 225\pm65$ ms
Counts
Counts
Counts
4000
2000
1000
800
600
400
10
1
10
1
0
500
1000
1500
2000
2500
3000
Time (ms)

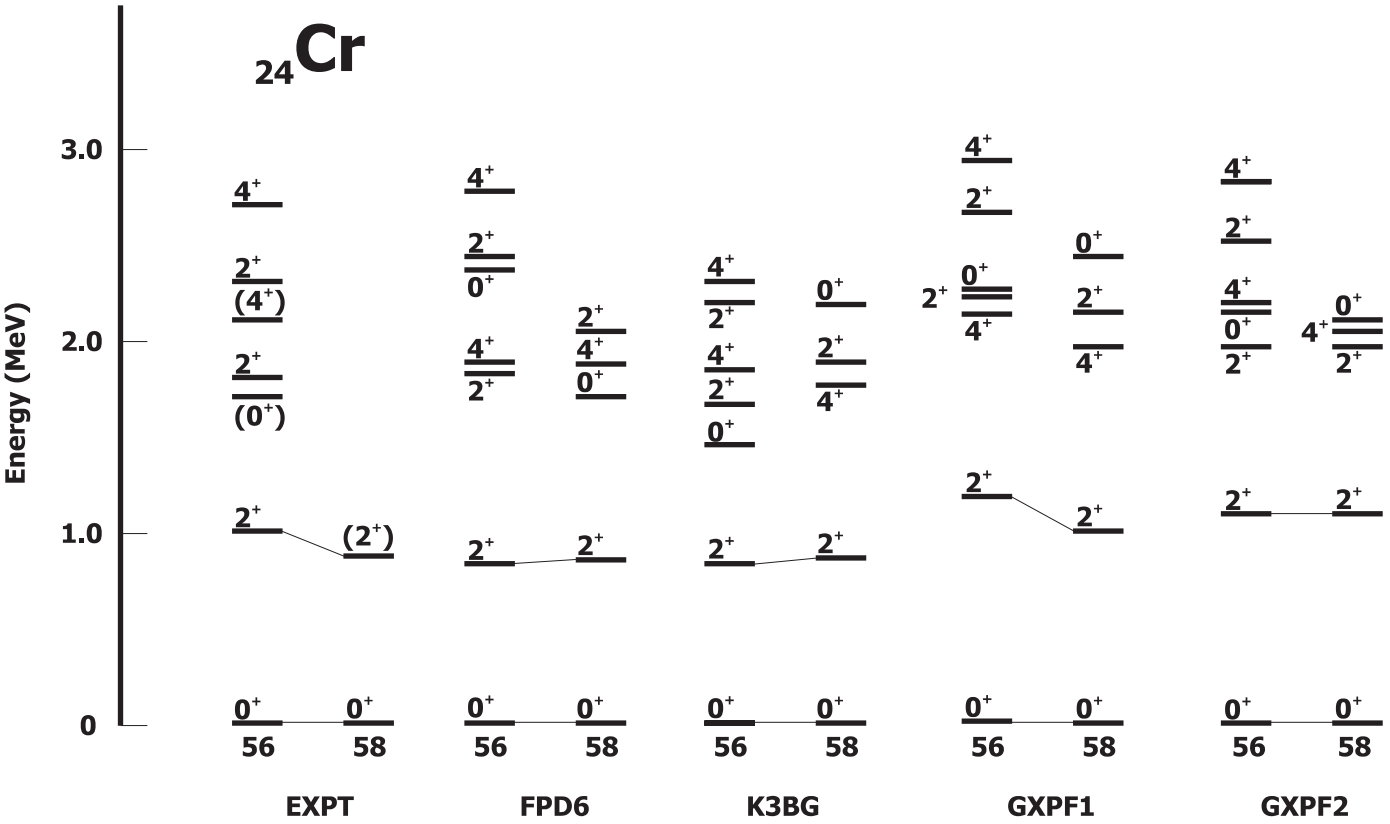
24Cr
Energy (MeV)
3.0
2.0
1.0
0
4+
2+
(4+)
2+
(0+)
2+
(2+)
0+
0+
56
58
EXPT
4+
2+
0+
4+
2+
0+
2+
2+
0+
56
58
FPD6
4+
2+
4+
2+
0+
2+
2+
4+
0+
56
58
K3BG
4+
2+
0+
2+
4+
4+
2+
2+
0+
56
58
GXPF1
4+
2+
0+
2+
4+
0+
2+
4+
2+
2+
56
58
GXPF2